Geotechnical and Geological Engineering, 1997, **15** 263–282

The shear strength of clay-filled bedding planes in limestones – back-analysis of a slope failure in a phosphate mine, Israel

Y.H. HATZOR* and M. LEVIN

Rock Mechanics Laboratory of the Negev, Department of Geological and Environmental Sciences, Ben-Gurion University, Beer-Sheva, 84105, Israel

Received 12 June 1997
Accepted 29 August 1997

Summary

The failure of a slope in a phosphate mine by shear-sliding along a clay-filled bedding plane in limestone, and by separation across a tension crack at the back, is back-analysed. The failure cannot be explained using laboratory measured values of the shear strength parameters. In order to simulate field conditions better two 'physical models' of the bedding plane were prepared for testing under triaxial compression. Cylindrical cores with an inclined saw-cut discontinuity were filled with remoulded montmorillonite. It is shown that failure in the models initiates along the contacts between the clay infilling and the limestone boundaries, and not through the clay itself, as would be intuitively expected. Furthermore, it is argued that in the analysis of rock slope stability in general, and particularly in the case of clay-filled discontinuities, the influence of paleo-overburden stress on frictional resistance must be resolved before the appropriate constitutive law can be established for analysis.

Keywords: Rock slope stability; plane failure; shear strength; stiff clays; montmorillonite; back analysis.

Introduction

The stability of a rock slope containing an inclined plane of weakness has been discussed by many authors, including Terzaghi (1962), Jaeger (1971), Goodman (1976), Hoek and Bray (1981), Wittke (1990), and West (1996), among others. The first and foremost requirement for instability is that the rock slope consists of a finite and removable block. Rigorous determination of block removability requires application of Block Theory analyses as discussed by Goodman and Shi (1985) and demonstrated by Hatzor (1993) and Hatzor and Goodman (1997). However, in routine mining applications, to ensure that the block is finite, it is sufficient to establish that the block is separated from the rock mass by

* To whom correspondence should be addressed.

a so-called 'tension crack' and by two transverse discontinuities, sub-parallel and sub-perpendicular to the free face of the excavation respectively. A kinematic removability criterion in such a setting is that the plane of weakness must daylight, namely, the dip of the sliding plane must be smaller than the dip of the free face.

A block which is free to slide out of the rock mass by virtue of kinematics is safe as long as the available shear strength of the sliding plane is greater than the driving shear stress, provided that no tensile and shear resistance are supplied by the boundary joints. The available shear strength of discontinuities in general, including bedding planes, has been investigated extensively, and both theoretical and empirical constitutive laws have been developed. The most commonly used failure criterion to date is the empirical Mohr–Coulomb linear law which postulates that the shear strength of discontinuities consists of a normal stress-independent component – the 'cohesion', and a normal stress-dependent frictional component. While the cohesion intercept is routinely found in intact rock and soil materials, its role in the shear strength of discontinuities remains to be verified. Recently West (1996) has suggested that a source for apparent cohesion in rock discontinuities could be areas of intact rock along the discontinuity surface which must be sheared before sliding can ensue.

The Mohr–Coulomb criterion ignores the contribution of surface roughness to available shear strength, the significance of which has been discussed by Patton (1966), Ladanyi and Archambault (1970), Rengers (1970), Barton (1973), Bandis *et al.* (1983), Haberfield and Johnston (1994), and Hencher (1995) among others. While surface roughness is of supreme importance in the case of clean, tight, matching surfaces, particularly at the initiation of sliding and before residual strength is attained, the role of roughness becomes less important as the thickness of the infilling material increases. Goodman (1970) and Ladanyi and Archambault (1977) in a series of direct shear tests on filled-dilatant joints have shown that when the filling thickness is greater than the joint roughness amplitude by a factor of 1.5, the shear strength of the discontinuity is dictated by the shear strength of the infilling material.

In this paper, the shear failure of a large rock slope along a clay-filled bedding plane in limestones is back-analysed. The shear strength of both the clay infilling and the clay–limestone contact is determined using consolidated drained (CD) direct shear tests, as well as triaxial tests.

Description of the failure

During the dry month of August, 1994, a large rock block, 40 m high, 30 m wide and with a length along strike of 55 m, slid a distance of 5 m along a bedding plane dipping 19° into the excavation space, following exposure of the sliding plane by excavation activities at the foot of the slope. The failure took place in the Arad phosphate open-pit mine in southern Israel, a mining site which is developed along the SE dipping flanks of a NE striking anticline (Fig. 1). The original slope dip was 56° and the sliding mass consisted of phosphatic limestone at the base, phosphate layers (the ore), marly chalk, and alluvium at the top (Fig. 2). As a result of the failure, the tension crack developed to a channel 5 m wide which was quickly filled with debris, and several new parallel tension cracks developed at the newly developed free surface. At the foot of the sliding mass, ground

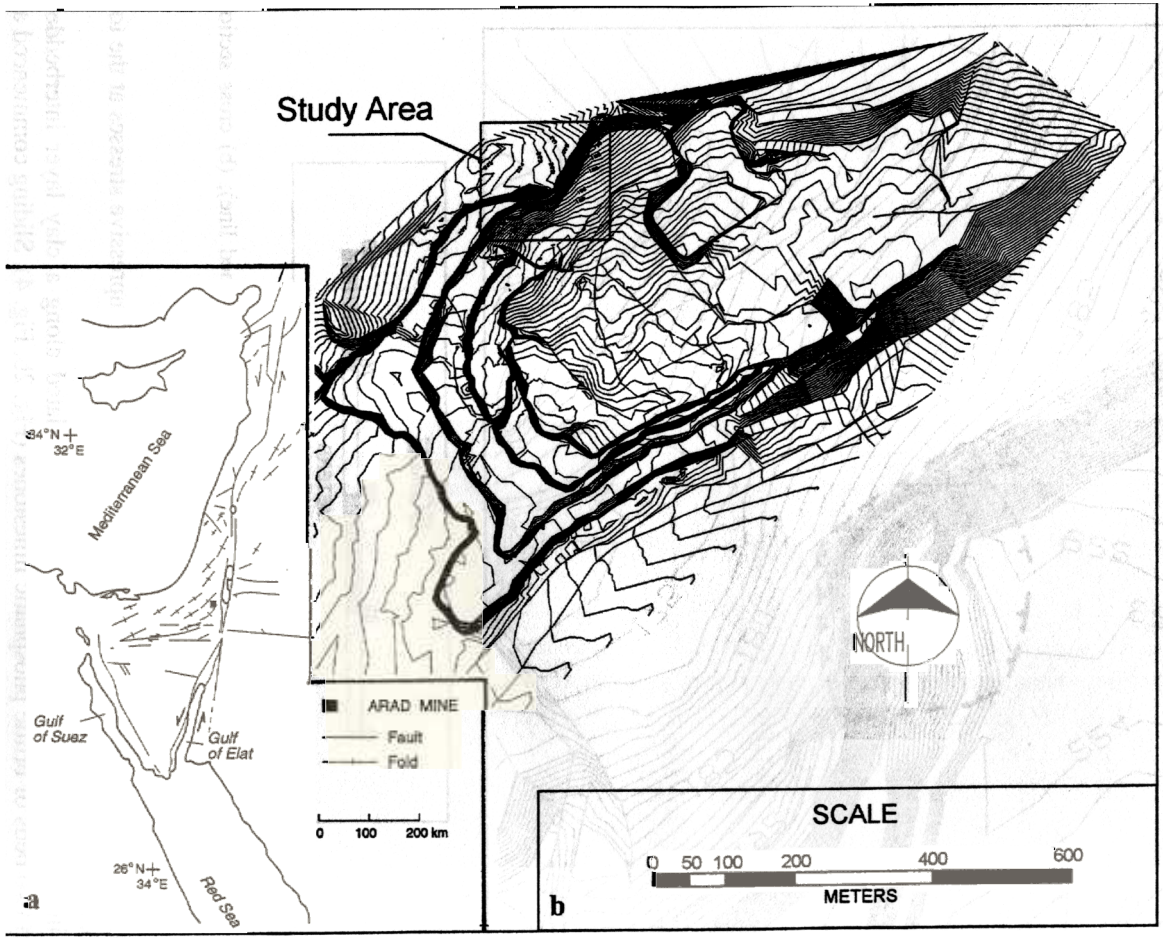

Fig. 1. Location map of the studied area. (a) Regional location map (after Garfunkel, 1981); (b) topographic contour map of Arad mine (Courtesy Rotem Amfert Negev, LTD).

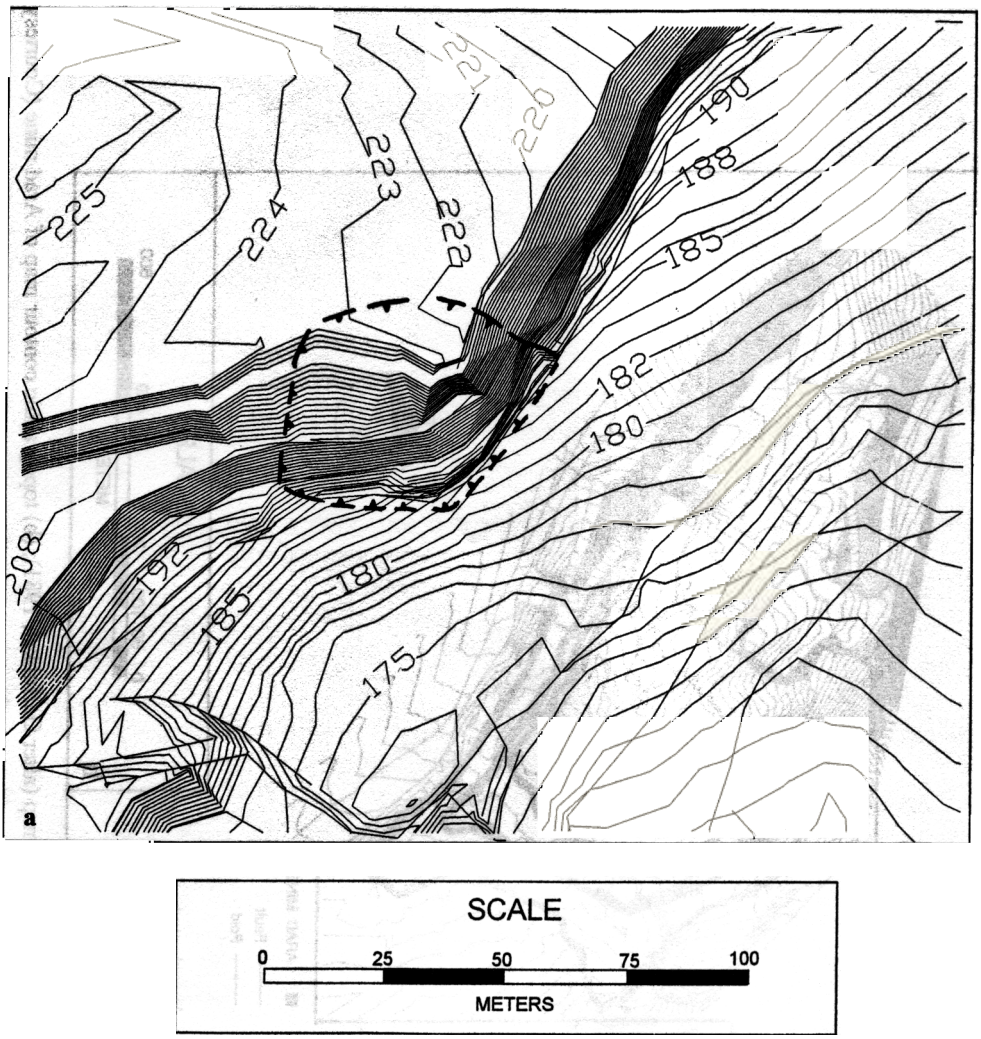

Fig. 2. (a) Topographic contour map of the failed slope (heavy dashed line); (b) cross section through the failed slope.

heave was detected coupled with axial splitting due to high compressive stresses at the toe (Fig. 3).

Site investigations revealed that sliding had initiated along a clay layer interbedded between two beds of brittle phosphatic limestones (Fig. 2b, Fig. 4). Sliding commenced as the clay layer was being exposed, and consequently the mining equipment was buried under the earth that was displaced at the foot of the slope.

No groundwater seepage was detected through the exposed sliding plane during or after the failure episode and it is therefore assumed that failure occured at zero cleft water pressure. Furthermore, seismological data from the date and time of the failure do not indicate any unusual activity in the vicinity of the mine (Geophysical Institute of Israel,

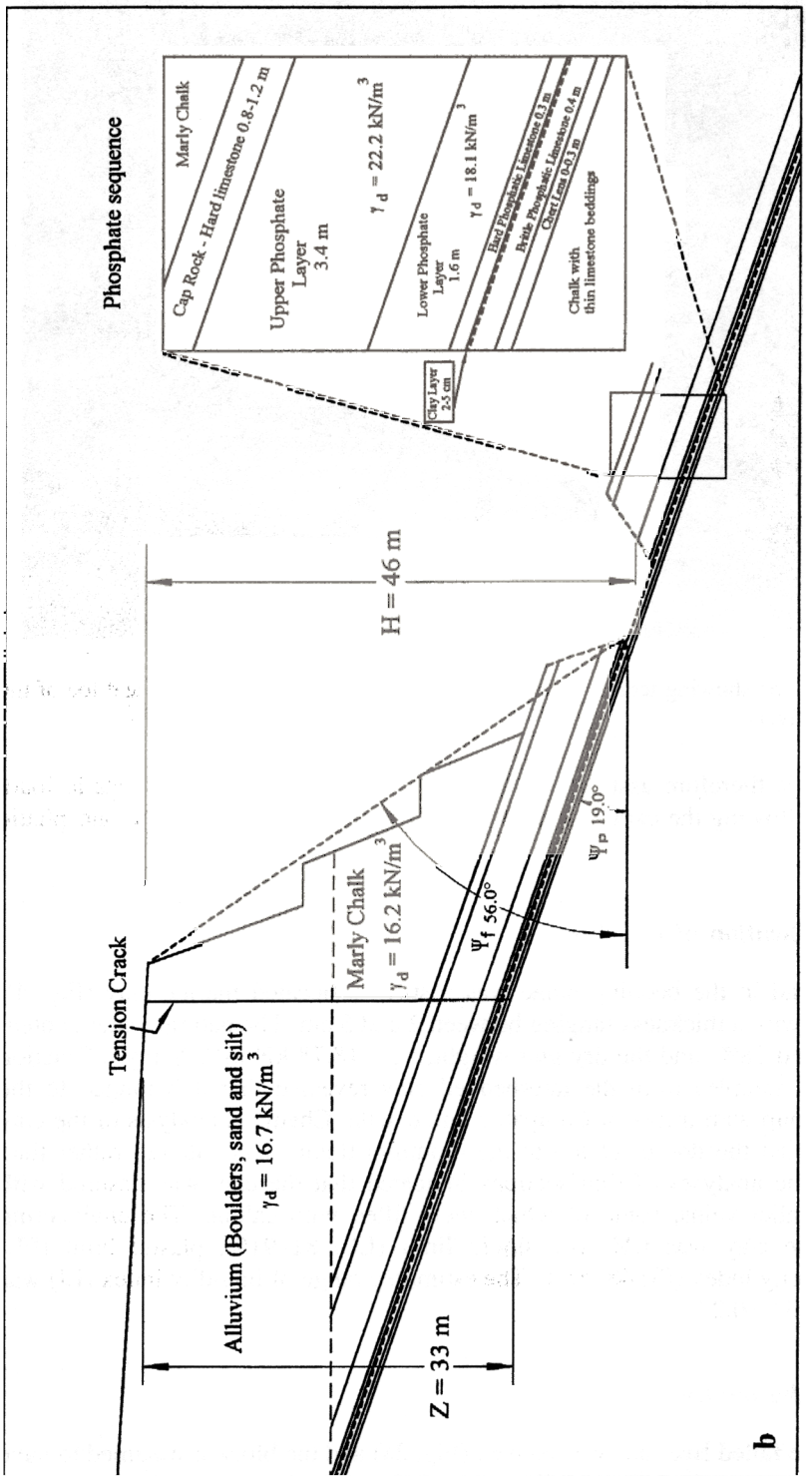
Phosphate sequence
Marly Chalk
Cap Rock - Hard limestone 0.8-1.2 m
Upper Phosphate Layer 3.4 m
γ_d = 22.2 kN/m^3
Lower Phosphate Layer 1.6 m
γ_d = 18.1 kN/m^3
Bed Phosphatic Limestone 0.3 m
Pebbly Phosphatic limestone 0.4 m
Chert Layer 0.0.3 m
Chalk with thin limestone beddings
Clay Layer 2.5 cm
H = 46 m
Tension Crack
Alluvium (Boulders, sand and silt)
γ_d = 16.7 kN/m^3
Marly Chalk
γ_d = 16.2 kN/m^3
Ψ_f 56.0°
Ψ_p 19.0°
Z = 33 m
b

Fig. 2. (b).

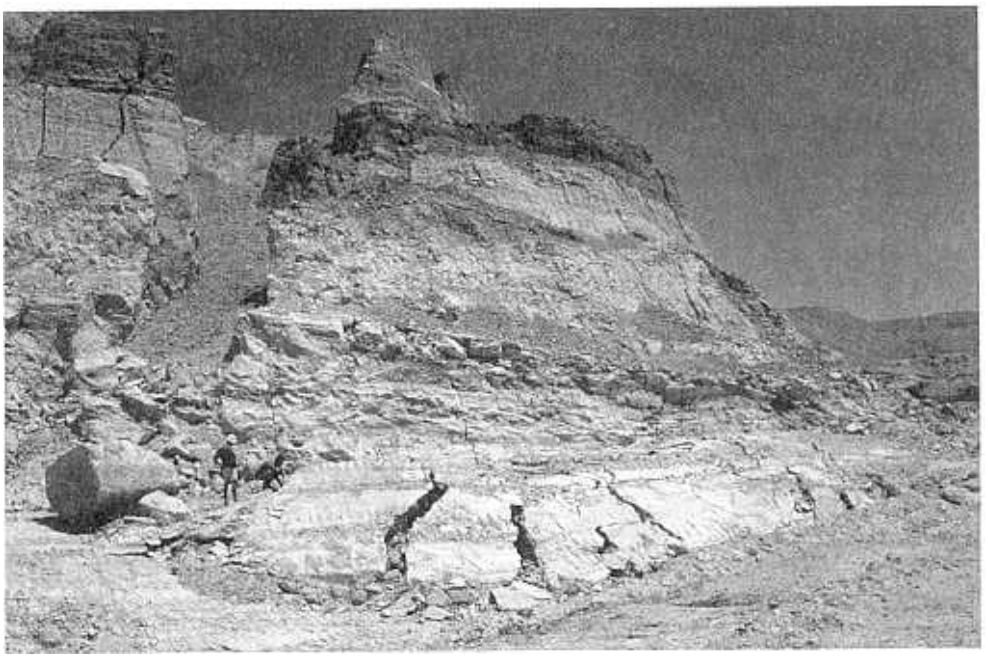

Fig. 3. The failed slope showing tensile and compressive deformations at the head and toe of the sliding block, respectively.

1994). The failure is therefore assumed to be the result of instability under static load, which developed following the exposure of the clay-filled bedding plane in the phosphatic limestones.

Engineering classification of the clay

The infilling material in the bedding plane was a stiff, desiccated marine clay (Fig. 4), dark-brown to red, with a thickness ranging between 2 and 5 cm. The natural water content was between 9% and 18%, and the dry unit weight, $\gamma_d = 18.78$ kN m^{-3}. X-ray diffraction (XRD) analyses of samples from the interbedded clay revealed that it belonged to the montmorillonite group with traces of Ca-apatite and calcite. Chemical analysis of the clay material indicated that the dominant ion in the montmorillonite was calcium rather than sodium. Petrographic analyses of thin sections indicated that the clay was fissured with many thin and parallel veins, some of which were filled with calcite. The engineering classification of the clay was CH with liquid limit (LL) 81–91%, plastic limit (PL) 33–35%, and plasticity index (PI) 48–56%. The estimated range of liquidity index (LI) was between -0.54 and -0.27.

Back analysis of the failure

The geometry of the failed free face was convex (Fig. 2a) and the block is assumed to have been free of side forces at the time of failure. The failure can therefore be back-analysed

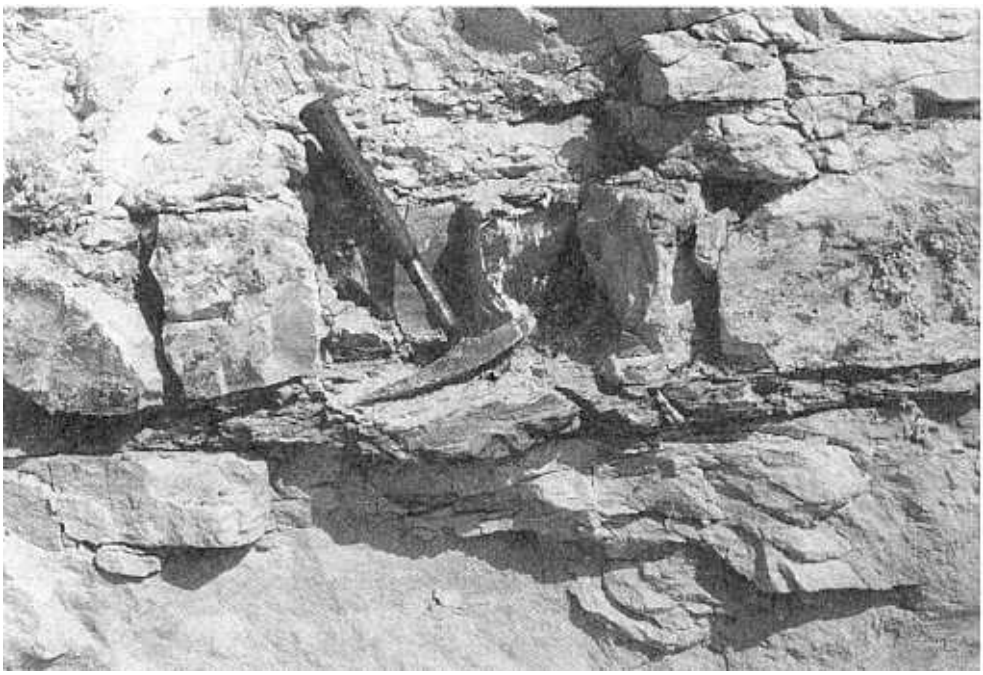

Fig. 4. Detail of the interbedded, stiff, marine, clay layer.

quite accurately using a simple two-dimensional analysis, provided that block dimensions and unit weights are known. A great effort was made to retrieve the exact geometry of the failed block, using an electronic distance meter (EDM) and careful geological mapping. The dimensions and weights which were used in the analysis are shown in Fig. 2b. The stratigraphic sequence starts at the base with chalk, chert and limey phosphatic layers. The main phosphatic rock unit consists of 1.6 m of organic phosphates (lower phosphate, $\gamma_d = 18.1$ kN m^{-3}) and 3.4 m of phosphatic limestone (upper phosphate, $\gamma_d = 22.2$ kN m^{-3}), covered with 1 m of hard phosphatic limestone (cap rock). Above the phosphatic rock units there were 10–15 m of marly chalk ($\gamma_d = 16.2$ kN m^{-3}), and 17–20 m of alluvium which consisted of conglomerates, boulders and gravel with a silty sand matrix (estimated dry unit weight $\gamma_d = 16.7$ kN m^{-3}). The base of the alluvial material was formed of original deposits while the top consisted of excess material from earlier mining.

The factor of safety against single plane sliding in the general case of a saturated slope is given by (e.g. Hoek and Bray, 1981):

$$F = \frac{cl + (W\cos\psi_p - U - V\sin\psi_p)\tan\phi}{W\sin\psi_p + V\cos\psi_p} \tag{1}$$

where c = cohesion across the sliding plane, l = length of the sliding plane, W = overall weight of the sliding block, U = resultant water force acting on the sliding plane, V = resultant water force acting on the tension crack, ψ_p = dip angle of the sliding plane, and ϕ = friction angle of the sliding plane. In our case sliding is assumed to have taken place under dry conditions and therefore U and V are zero. The length of the sliding plane

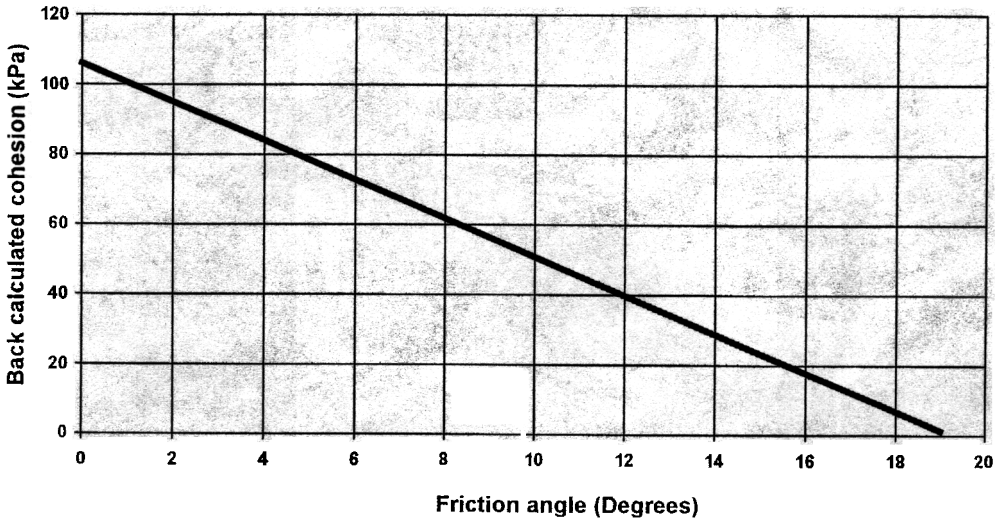

Fig. 5. Results of two-dimensional back–analysis of the sliding block.

(l) is 40 m, the calculated weight of the sliding block (W) is 12 926 kN, and the average dip of the sliding plane (ψ_p) is 19°. In order to back-analyse the failure, a factor of safety is assumed to be 1.0 at the point of failure. The back-analysed strength parameters of the sliding plane (c, ϕ) are dependent upon each other in this method, the dependence of which is found when a value of 1.0 is substituted for F in Equation 1 for the dry case:

$$c = \frac{W \sin \psi_p - W \cos \psi_p \tan \phi}{l} \tag{2}$$

The graphical solution for this relationship is shown in Fig. 5. It is shown that the maximum values of back calculated cohesion and effective friction angle must not be greater than 105 kPa and 19° respectively. Recalling that the average dip of the sliding plane is 19°, the solution of $c = 0$, $\phi = 19°$ seems to explain the failure perfectly well. This solution is intuitively appealing because the bedding plane upon which sliding took place appears to be open in the field, with apparent gaps between the clay and the limestone (Fig. 4). Cohesion therefore is not expected to be mobilized while the contact between the stiff desiccated clay and the overlying limestone is being sheared.

In order to validate the back-calculated strength values of the sliding plane the clay was tested in CD direct shear, and the clay–limestone contact was tested both in CD direct shear and triaxial shear tests, the results of which are described below.

Shear strength of the clay-filled bedding plane

Residual friction angle of clean bedding planes

Field investigations have clearly revealed that sliding took place along the clay filled bedding plane in the phosphatic limestone (Figs 2 and 4). In order to remove any doubt

Table Results of tilt tests performed on polished contacts

Sample	Average $\phi_{residual}$ (degrees)	Minimum $\phi_{residual}$ (degrees)	Contact between:
	25.6	23	Hard phosphate – chert
	23.8	22	Hard phosphate – chert
	28.7	27	Lower phosphate – hard phosphate
	28.4	25	Lower phosphate – hard phosphate
	33	31	Lower phosphate – hard phosphate
	30.8	29	Lower phsophate – chert
	29.2	27	Lower phosphate – hard phosphate
	32.5	29	Lower phosphate – chert

concerning the weakest surface in the stratigraphic sequence, tilt tests of eight polished stratigraphic contacts were performed, such that the residual friction angles between clean bedding planes with no infilling material could be determined. The contacts were surface ground to a roughness of 0.01 mm, since residual friction was assumed to be mobilized at the time of deformation, due to the large size of the overriding block. The tested contacts belong to three categories (Fig. 2): (a) contact between hard phosphatic limestone and the chert member (samples AR1, AR2); (b) contact between hard phosphatic limestone and lower phosphate member (samples AR3, AR4, AR5, AR7); (c) contact between brittle phosphate and the chert member (samples AR6, AR8). Ten tilt tests were performed for each sample, and the average and minimum values of the residual friction angles are listed in Table 1.

The results of all tilt tests clearly show that the available residual friction angle is sufficient to avoid shear failure. Therefore the remaining validation effort of the back-analysed strength parameters must concentrate on the clay-filled bedding plane.

CD direct shear tests on the clay

Consolidated drained direct shear tests of 'undisturbed' samples of the clay, retrieved in the field using a 63.3 mm core barrel, were performed at the geotechnical lab of the Technion, Israel. The field values of normal and shear stresses which acted upon the failure plane (at failure) were calculated to be $\sigma_n = 306$ kPa and $\tau_{mobilized} = 105$ kPa, respectively. In order to test the clay at a representative normal stress range, four cylindrical specimens, with nominal diameter of 6.33 cm and height of 2.45 cm, were saturated and consolidated under normal stress values of 49 kPa, 216 kPa, 436 kPa, and 660 kPa. After saturation the samples exhibited some axial strain as shown in Table 2 (positive values indicate axial swell). Following consolidation, the samples were sheared under drained conditions at a horizontal displacement rate of 0.014 mm min^{-1}. Some physical properties of the samples tested are listed in Table 2. The resulting stress–strain curves are shown in Fig. 6, where the test under $\sigma_n = 660$ kPa is not shown because the required shear force was greater than the capacity of the load cell which was used.

The results of the three tests are plotted in a Mohr–Coulomb diagram in Fig. 7. The cohesion intercept is at 578 kPa and the best linear fit for the three tests yields an effective

Table 2. Physical properties of the tested Ca-montmorillonite before and after CD direct shear tests

Normal stress, σ_n(kPa)	49	216	436	660
Initial water content, w (%)	18.6	14.1	14.1	14.1
Initial dry density, ρ_d kg m^{-3}	1852	1932	1940	1917
Final dry density, ρ_d kg m^{-3}	1782	1857	1850	1787
Axial strain after saturation (%)	3.9	4.0	4.8	7.3

friction angle of 19.2°. At a normal stress value of 300 kPa (the average normal stress which acted upon the failure surface at failure), the available shear strength of the clay is in the order of 680 KPa, 6.5 times greater than the mobilized shear stress which was calculated ($\tau_{mobilized}$ = 105 kPa). Clearly failure could not have developed through the clay infilling, if we assume the laboratory test results are valid. The remaining surface of weakness which must be tested therefore is the contact between the clay and the limestone.

CD direct shear tests of the clay–limestone contact

In order to test the clay–limestone contact, a 6.33 cm diameter composite sample was prepared for CD direct shear, consisting of a 1.45 cm high clay cylinder at the base, and a 2.03 cm high limestone cylinder at the top. The initial dry density (ρ_d) and water content (w) of the clay were ρ_d = 1914 kg/m^3 and w = 9.6%. Both ends were polished to obtain a smooth contact between the limestone and the clay, at the same level as the ends of the upper and lower ring. Two 'multiple stage' direct shear tests, at a constant horizontal displacement velocity of 0.07 mm min^{-1}, were performed under normal stress values of σ_n = 49 kPa, 216 kPa, and 436 kPa: one at natural water content and another at saturation. In the 'dry' case, the sample was sheared three times, starting in each stage from zero horizontal displacement and the appropriate normal stress value, without extracting the sample. In the second set of tests the sample was saturated and consolidated under the same three normal stress values as in the first ('dry') case. Due to saturation the samples exhibited some volume change which resulted in axial elongation or shortening, and therefore after each shearing stage the lower cylinder was extracted, re-polished, and fitted properly into the ring again for the next stage. Stress–strain curves for all six test stages are shown in Fig. 8. One interesting result is that the contact at saturation presents higher peak stresses and exhibits a clear transition from peak to residual strength.

Three failure envelopes for the clay–limestone contact are shown in Figure 7. The saturated case exhibits a higher friction angle value (ϕ' = 35°) and an apparent cohesion, while the 'dry' case exhibits zero cohesion and a slightly lower friction angle (ϕ' = 32°). Considering the fact that the composite sample consists of a pre-existing, open, discontinuity (the polished contact), the apparent cohesion inferred from the cohesion intercept in the saturated case should not be considered a true material property.

For validation study, the results of the *residual* strength values (open circles in Fig. 7) would be the most representative of the *in situ* conditions. Considering a normal stress

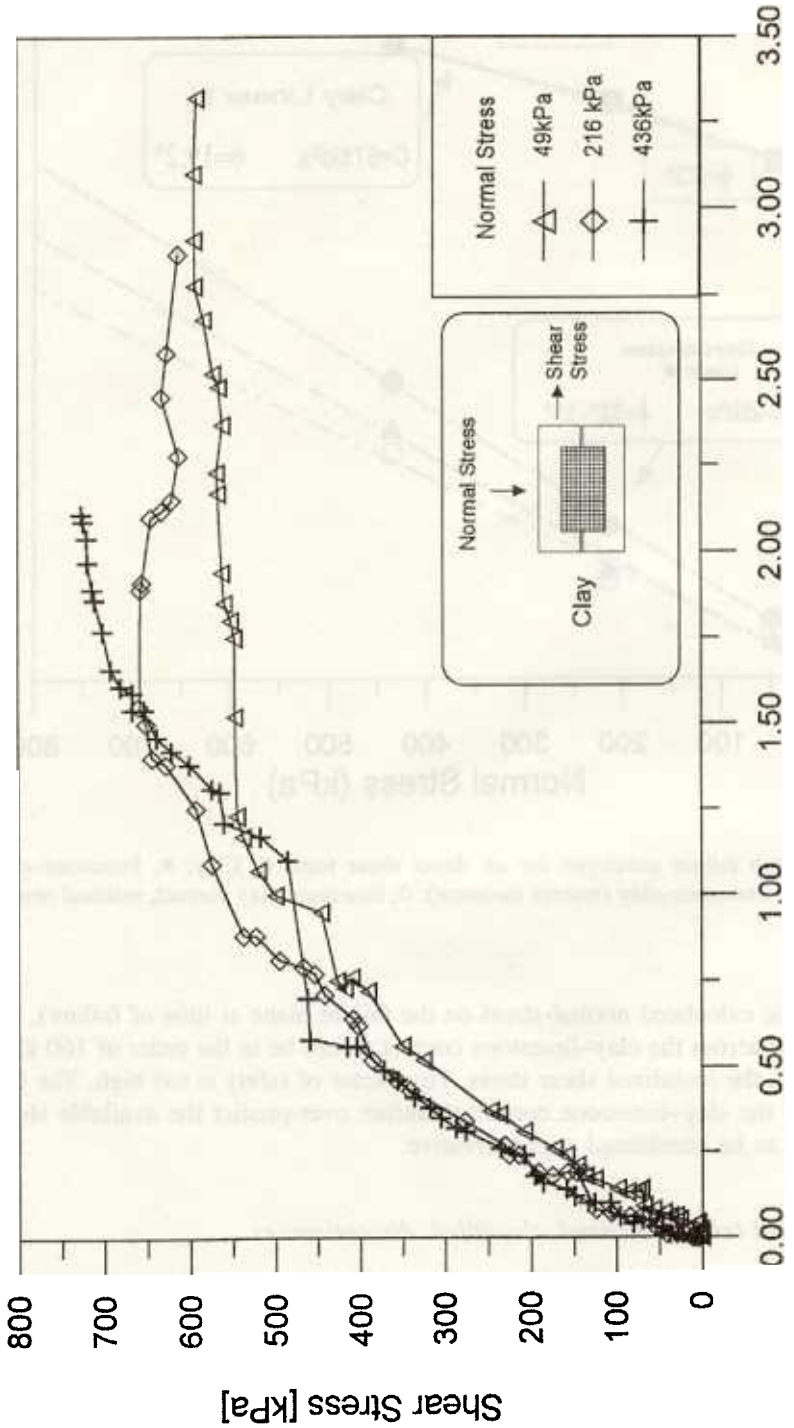

Fig. 6. Stress–strain curves for three direct shear tests of the interbedded Ca-montmorillonite.

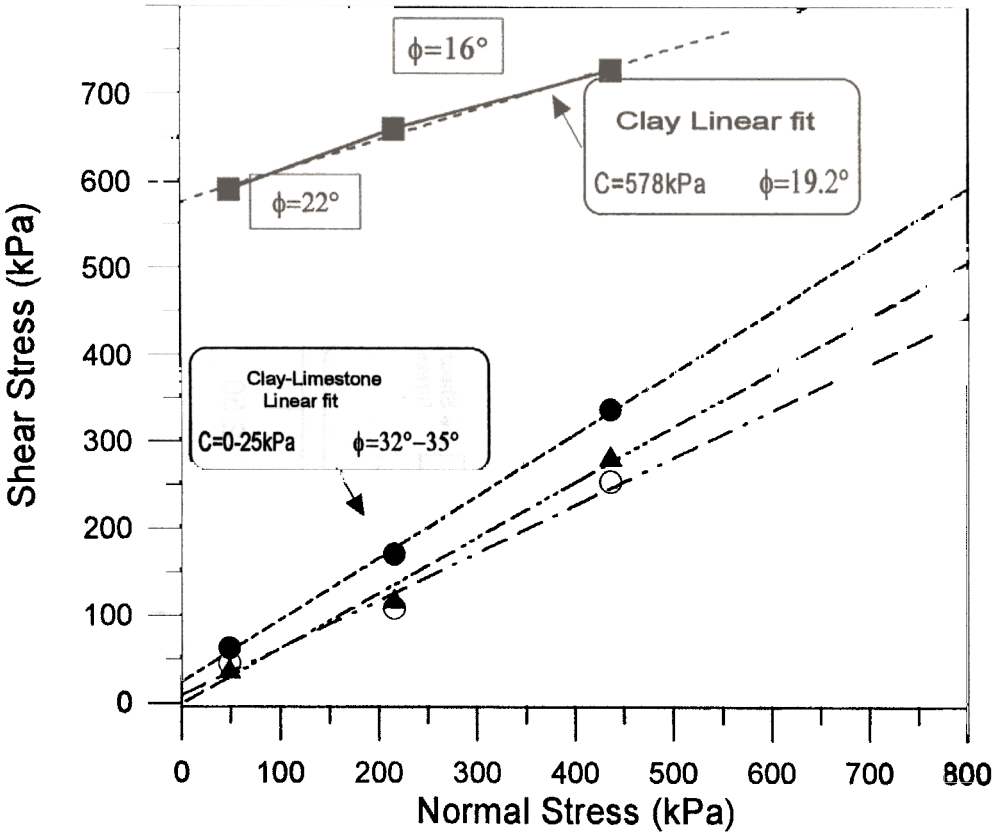

Fig. 7. Mohr–Coulomb failure envelopes for all direct shear tests. ■, Clay; ●, limestone–clay contact (saturated); ▲, limestone–clay (natural moisture); ○, limestone-clay contact, residual results (saturation).

value of 300 kPa (the calculated normal stress on the failure plane at time of failure), the available shear stress across the clay–limestone contact would be in the order of 160 kPa, 1.5 times higher than the mobilized shear stress. This factor of safety is too high. The CD direct shear tests of the clay–limestone contact therefore over-predict the available shear strength, and ought to be considered unconservative.

Multiple-stage triaxial tests of inclined, clay-filled, discontinuities

The CD direct shear tests of the clay–limestone contact were performed under normal stress values similar to the current vertical *in situ* stress. The results thus obtained suggest that the available shear strength was greater than the mobilized shear stress at time of failure. Since the block did slide however, an alternative method was devised in order to evaluate better the available shear strength in the laboratory. In particular the influence of stress history, or paleo-overburden stress, on the shear strength of the clay-limestone

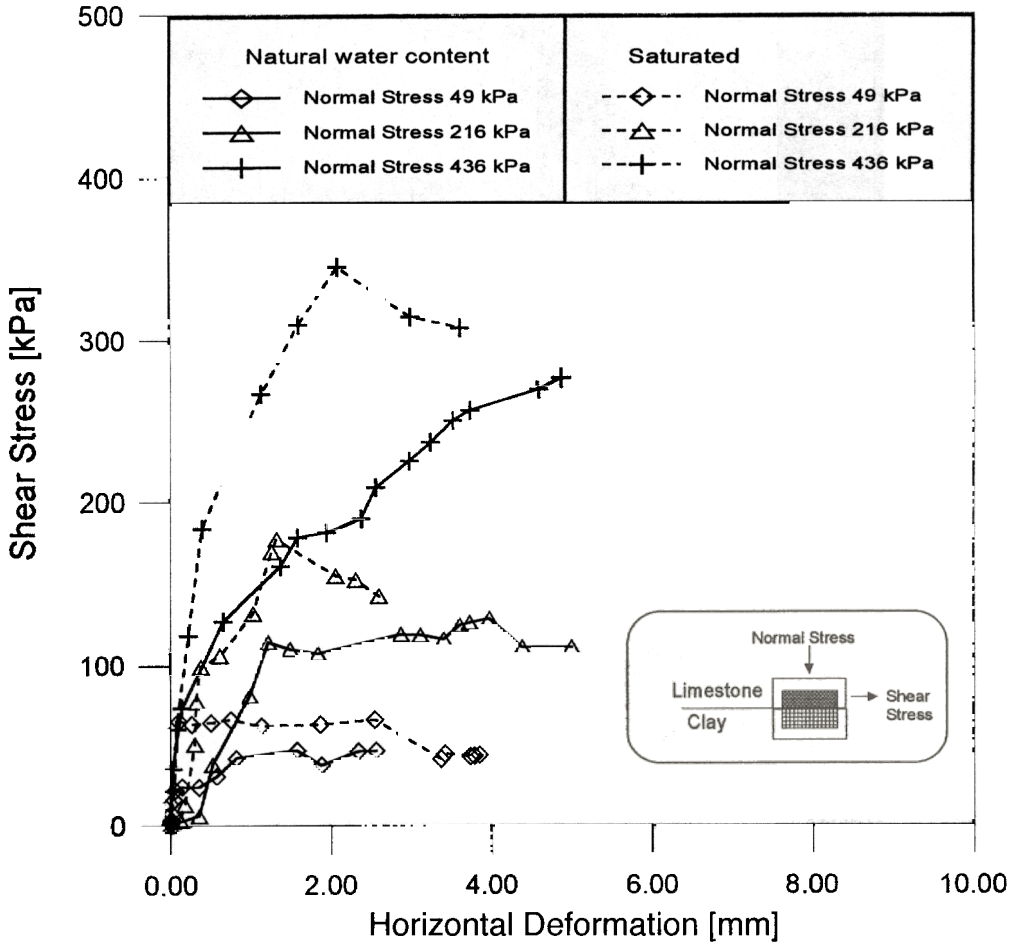

Fig. 8. Stress–strain curves for the clay–limestone contact.

contact was studied by subjecting the contact to confining pressures greater than the current *in situ* vertical stress.

Two solid cylinders of 54 mm diameter with a length-to-diameter ratio of 2.0 were prepared from the phosphatic limestone for triaxial testing, according to stringent ASTM and ISRM standards concerning end roughness, which did not exceed 0.01 mm. The solid cylinders were saw cut at an angle of 40° with respect to their axis, such that the normal to the discontinuity plane was inclined at 50° to the axial load direction. The saw-cut surfaces were first polished and then filled with moist, remolded, clay which was sampled from the sheared bedding plane in the field, thus obtaining a 'physical model' of the failure plane. The 'models' were jacketed by shrink tubes (ALPHA FIT-221-3) after the specimen ends were fitted parallel to one another. Axial deformation was monitored using a four-arm strain cantilever system which was mounted on the lower end-cap. The deflection of the arms against a deflection cone, mounted on the upper end cup, was calibrated for axial

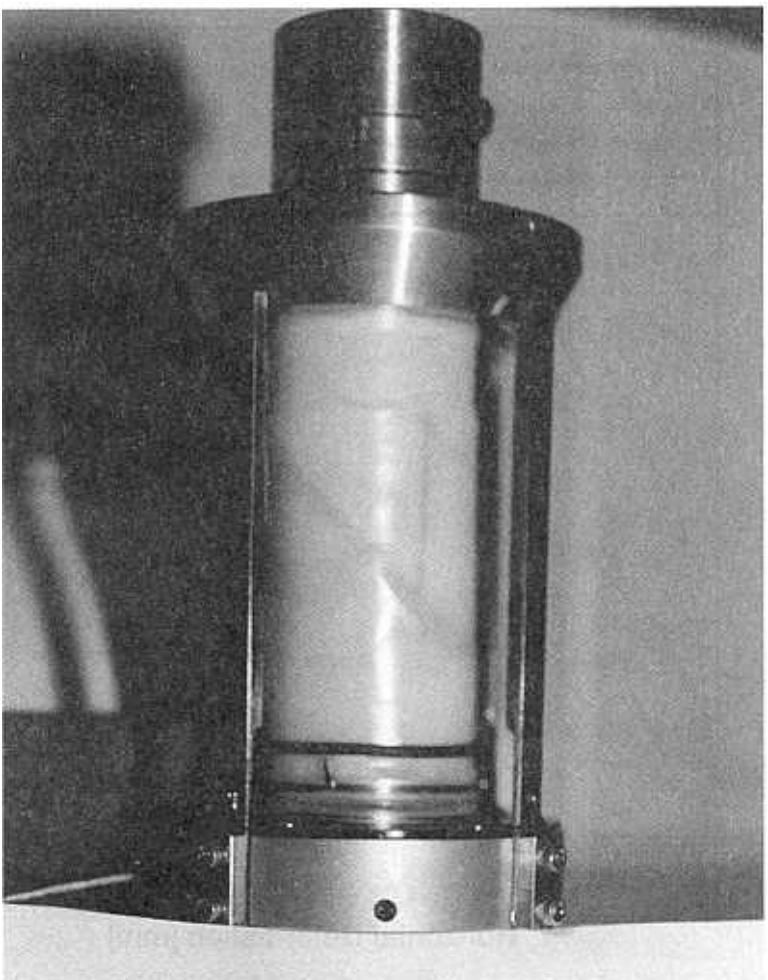

Fig. 9. (a) Inclined, clay-filled, discontinuity, with axial strain cantilever set mounted on the NX size sample for triaxial compression; (b) model of clay-filled discontinuity after triaxial shear.

displacement thus ensuring that axial strain readings represent axial deformation along the entire sample length (Fig. 9a). All triaxial tests were performed at the rock mechanics laboratory of BGU.

The samples were first subjected to all around hydrostatic compression, one sample at $\sigma_{3o} = 3$ MPa (sample AR11), and the other at $\sigma_{3o} = 15$ MPa (sample AR10). After initial hydrostatic compression, the confining pressure was reduced to zero, and then a multiple-stage triaxial test was performed. Each stage consisted of increasing the confining pressure from zero to a pre-determined value, applying a constant strain rate at $+1 \times 10^{-5}$ sec^{-1} (positive indicates compression) from zero axial strain up to the onset of stick slip oscillations at peak stress, quick axial strain-rate reversal at -1×10^{-5} sec^{-1} (unloading) from peak to zero stress difference, and confining pressure increase to the next pre-

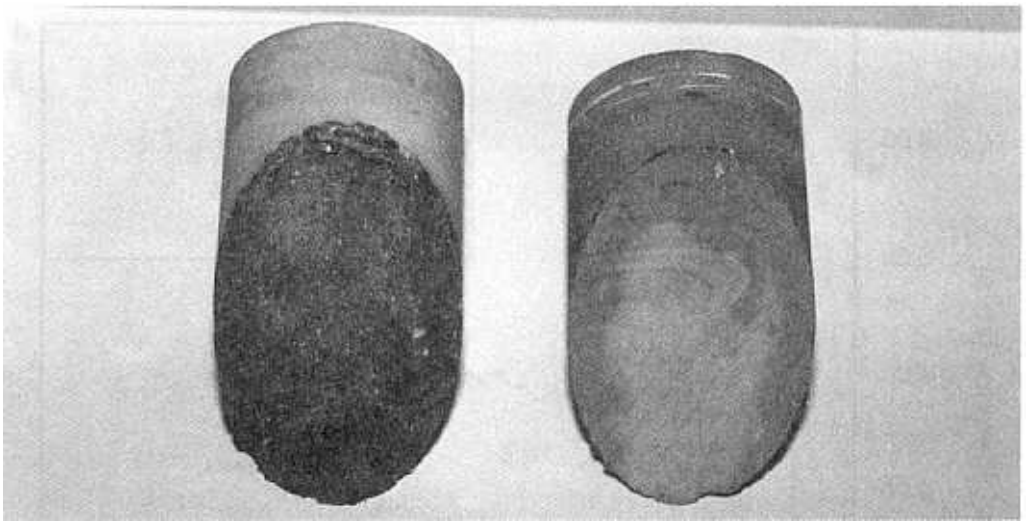

Fig. 9. (b).

determined level. Piston displacement was monitored using closed loop servocontrol, where the displacement signal was read from a high sensitivity LVDT placed outside the pressure vessel. Load was monitored using a 222 KN load cell with linearity of 0.5% full scale, which was placed directly below the sample stack. The load frame (TerraTek Systems model FX-33090) had a stiffness of 10^9 kN m^{-1}.

Stress–strain curves for the two multiple-stage triaxial tests are shown in Fig. 10. The sample which was pre-consolidated under initial confining pressure of $\sigma_{3o} = 3$ MPa (AR11) exhibits smooth transition from elastic deformation to shear sliding. Strain hardening behaviour is indicated under higher confining pressure values ($\sigma_3 = 2.8$ MPa, 4.72 MPa). Sample AR10, pre-consolidated under $\sigma_{3o} = 15$ MPa exhibits a relatively sharp transition from elastic deformation to shear sliding. Stick slip oscillations are detected at higher confining pressure values ($\sigma_3 = 3.3$ MPa, 5.7 MPa, 8.1 MPa).

Shear and normal stresses at failure on the saw-cut, inclined, clay-filled, discontinuity (σ_{nf}, τ_{ff}) were calculated for each confining pressure value from the stress–strain curves in Fig. 10, using the measured peak stress difference in each segment, the level of confining pressure, and the orientation of the discontinuity. The results are plotted in Fig. 11 in a shear-stress, normal-stress space. Both multiple stage tests follow a Mohr–Coulomb linear law at the tested normal stress levels. Linear regressions through each set of test results yield the following Mohr–Coulomb laws for the inclined discontinuities:

$$\sigma_{3o} = 3 \text{ MPa: } \tau = 0.16 + 0.32\sigma \ (c = 0.16 \text{ MPa; } \phi' = 17.7°; \ R^2 = 0.9943) \quad (3)$$

$$\sigma_{3o} = 15 \text{ MPa: } \tau = 0.26 + 0.24\sigma \ (c = 0.26 \text{ MPa; } \phi' = 13.5°; \ R^2 = 0.9963) \quad (4)$$

The apparent cohesion is meaningless since the tested discontinuity was open before and after the test; it stems from the mathematical representation of the data using a linear law. The friction angle values suggest that with relatively little 'pre-consolidation' the contact exhibits a friction coefficient which is just slightly insufficient for stability (ϕ' required = 19°, ($\phi' = 18°$ for $\sigma_{3o} = 3$ MPa), factor of safety = 0.94). With increasing

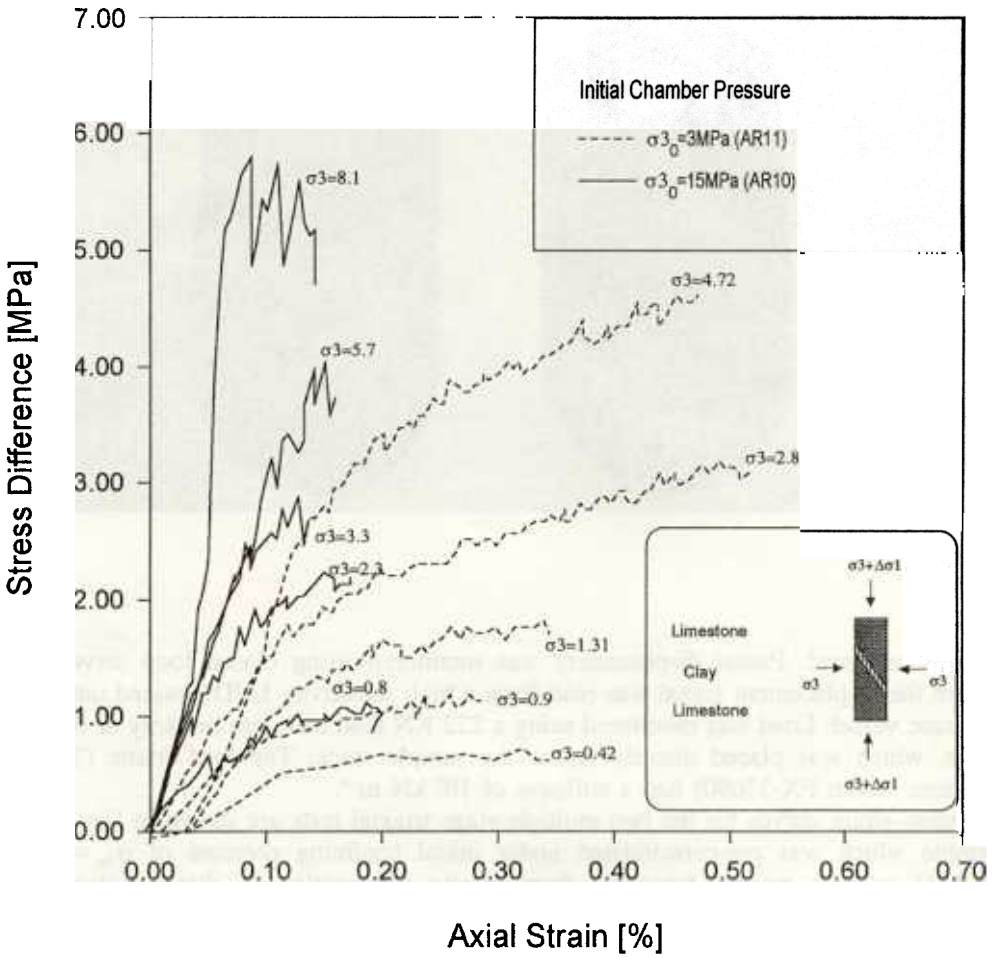

Fig. 10. Results of two multiple-stage triaxial tests on inclined, clay-filled, discontinuities subjected to two different levels of initial hydrostatic compression (σ_{3o}).

pre-consolidation the available friction angle further decreases to as low as $\phi' = 13.5°$ (for $\sigma_{3o} = 15$ MPa), and the factor of safety against sliding decreases to 0.69.

Discussion

Back analysis of the failure has indicated that the required cohesion and friction angle for stability were $c = 0$, $\phi' = 19°$ respectively. Due to careful geological mapping, and the well-defined geometry of the failed block, we believe these values represent limiting equilibrium conditions. Direct shear tests conducted on saturated samples from the Ca-montmorillonite infilling indicate that the cohesion of the clay is very high, of the order of 578 kPa, and that the effective friction angle is 19.2°. Although the available friction angle of the clay is identical with the required friction angle, we believe the measured cohesion

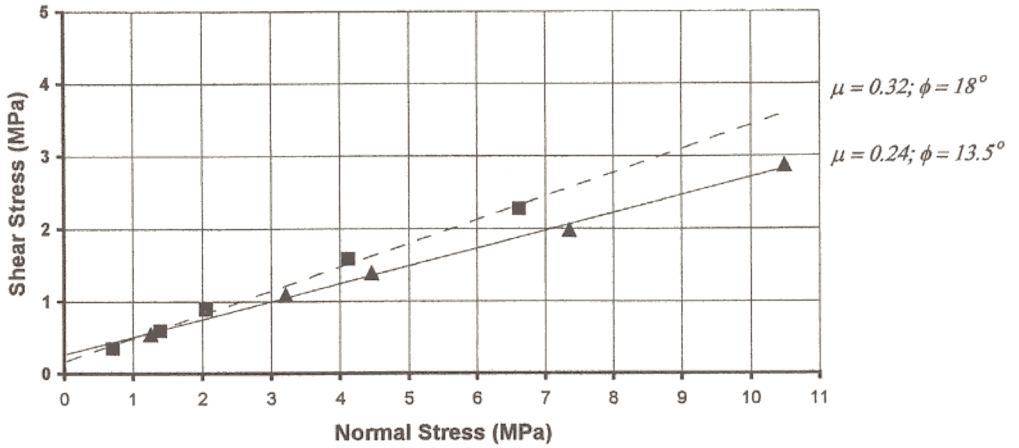

Fig. 11. Mohr–Coulomb failure envelopes for two multiple stage triaxial tests on clay-filled, inclined, discontinuities ($\beta = 50°$). ■, $\sigma_{3o} = 3$ MPa; ▲, $\sigma_{3o} = 15$ MPa.

is a valid material property. The factor of safety against shear through the clay therefore is about 6.5, assuming the normal and shear stresses across the failure plane at the time of failure were 306 kPa and 105 kPa respectively. A very intuitive geological engineering approach, in the analysis of the stability of such a rock slope, would be to focus the laboratory tests on the clay infilling. This case history illustrates that such an approach might be misleading, and in fact, unconservative.

An alternative approach would be to study the shear strength of the clay–limestone contact assuming residual strength due to the large size of the overriding block. This is done here using both saturated and dry CD direct shear tests of the contact. The cohesion thus obtained is negligible, but the residual effective friction angle is too high, $\phi'_{\text{saturated, residual}} = 32°$. Had this approach been taken by the geological engineer, the assumed factor of safety would have been 1.8, and the slope would have been considered safe.

Earlier workers (e.g. Goodman, 1976; Ladanyi and Archambault,1970, 1977) found that when the infilling thickness is greater than the roughness amplitude, the shear strength of the discontinuity is governed by the strength of the infilling. The results of this study indicate that shear commenced along the contact, although the thickness of the infilling was much greater than the discontinuity roughness amplitude. The discrepancy can be explained by the engineering properties of the stiff, marine clay which is studied here. Considering the negative liquidity index range and the fact that the natural water content is less than the plastic limit, the interbedded clay is expected to behave as a brittle solid (Holtz and Kovacs, 1981). When the infilling material consists of such a brittle material therefore, shear deformation may be achieved by shear through the contact asperities rather than by shear through the stiff clay.

Skempton and Petley (1967) studied similar stiff clays with similar liquidity index values ($-0.23 < \text{LI} < 0.19$) and tested both intact clays and pre-existing slip surfaces using both direct shear and triaxial tests. They found that the shear strength of pre-existing slip surfaces within the stiff clays was lower than shear strength of the intact clay. For a

variety of stiff intact clays they reported peak cohesion values between 2.8 and 47.9 kPa, and peak effective friction angles values between 18° and 24°. For a variety of slip surfaces within the same clays they reported residual cohesion values between 0 and 3 kPa and residual, effective friction angles between 12° and 16°. The results reported by Skempton and Petley (1967) show that pre-existing planes of weakness within stiff clays are weaker than the clay itself. Our results further demonstrate that when a discontinuity in hard rock is filled with a very stiff clay, the weakest plane is the contact between the stiff clay and the hard rock rather than a plane within the clay.

The true shear strength of the clay–limestone contact is lower than that measured in CD-direct shear tests and is shown here to depend upon the level of pre-consolidation, or paleo-overburden stress. Cylindrical samples containing inclined clay-filled discontinuities, subjected to initial hydrostatic compression (σ_{3o}) as a simulation of paleo-overburden stress, exhibit a dependence between frictional resistance and the magnitude of σ_{3o}. When a cylindrical sample was subjected to initial hydrostatic compression of $\sigma_{3o} = 3$ MPa, equivalent to paleo-overburden of 150 m (assuming $\gamma_d = 20$ kN m^{-3}), the measured friction angle of the contact was 18°, sufficiently low to explain the failure. When a similar sample was subjected to initial hydrostatic compression of $\sigma_{3o} = 15$ MPa, equivalent to paleo-overburden of 750 m, the measured friction angle of the contact was 13.5°.

It has been shown that the paleo-overburden does influence the frictional resistance of a clay–limestone contact using pre-compressed samples in conventional triaxial tests. Conventional direct shear tests are understood here to yield the frictional resistance of a contact which did not experience paleo-overburden, because unloading processes are inevitably associated with the sampling procedure. The influence of paleo-overburden stress on the frictional resistance of the contact is graphically demonstrated in Figure 12, where the direct shear tests are assumed to represent conditions of zero paleo–overburden.

Conclusions

In this paper a plane failure along a clay–filled bedding plane in limestones is back-analysed using careful geological mapping of the sliding block's geometry, and laboratory determination of unit weights. Thus the material properties of the failure plane required for limit equilibrium analysis are obtained with a great degree of confidence. Several conclusions emerge from the results:

(1) It is shown that the shear strength of the clay-filled bedding plane is dictated by the frictional resistance of the contact, rather than the shear strength of the clay. This result is in contrast to earlier findings, for example those of Goodman (1976) and Ladanyi and Archambault (1970, 1977) who found that when infilling thickness is greater than the roughness amplitude the shear strength of the discontinuity is governed by the strength of the infilling. The discrepancy could be a result of the great stiffness of the marine clay studied. Nevertheless, a rock slope stability analysis which is based on the assumption of shear failure through the clay could be erroneous, and as found here, unconservative.

(2) The shear strength of the clay-limestone contact is influenced by stress history, or the amount of paleo-overburden (σ_{3o}). Unloaded samples of the contact, retrieved

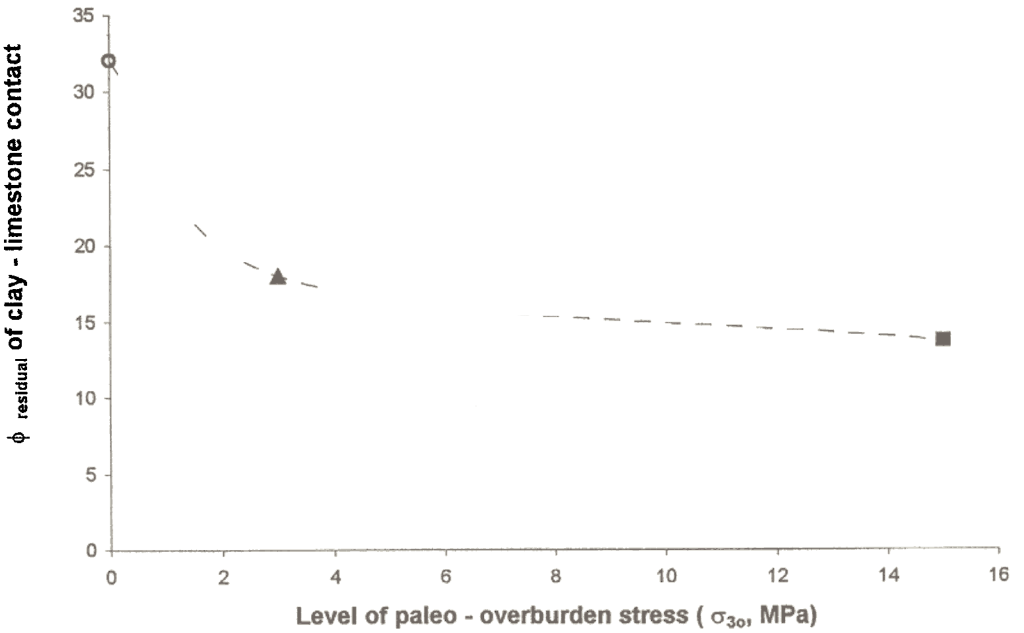

Fig. 12. Influence of paleo-overburden (σ_{3o}) on the frictional resistance of a stiff clay–limestone contact. ○, direct shear; ▲, triaxial shear; ■, triaxial shear.

during conventional sampling procedures in the field and tested in CD direct shear, exhibit higher frictional resistance than pre-compressed samples which are tested in triaxial shear. It is therefore necessary to test clay-filled discontinuities after pre-compression, at levels of σ_{3o} similar to the estimated paleo-overburden stress, in order to define the failure law better.

Acknowledgements

This research was funded by Rotem Amfert Negev LTD, a phosphates mining company, through contract No. 9-50-87505. E. Ron and Y. Levy of Rotem Amfert provided great help at the early phases of research and allowed free access to digitized mapping data and borehole data. A. Zur of Rotem Amfert provided help in the field and his help is acknowledged. Mrs H. Altshuler of the Technion Soil and Roads Laboratory assisted with sample preparation and direct shear testing and her careful work is acknowledged.

References

Bandis, S.C., Lumsden, A.C. and Barton, N.R. (1983) Fundamentals of rock joint deformation, *International Journal of Rock Mechanics, Mining Science and Geomechanical Abstract*, **20**, 249–68.

Barton, N.R. (1973) Review of a new shear strength criterion for rock joints, *Engineering Geology*, **7**. 287–332.

Garfunkel, Z. (1981) Internal structure of the Dead Sea leaky transform (rift) in relation to plate kinematics, *Tectonophysics*, **80**, 81–108.

Geophysical Institute of Israel (1994) *Seismological Bulletin of Israel and Adjacent Areas.*

Goodman, R.E. (1970) *The Deformability of Joints – Determination of the* In Situ *Modulus of Deformation of Rock*, ASTM STP 477, American Society for Testing Materials, Philadelphia, pp. 174–96.

Goodman, R.E. (1976) *Methods of Geological Engineering in Discontinuous Rocks*, West Publishing Company, St Paul.

Goodman, R.E. and Gen-Hua Shi. (1985) *Block Theory and its Application to Rock Engineering*, Prentice-Hall, Englewood Cliffs, NJ.

Haberfield, C.M. and Johnston, I.W. (1994) A mechanically-based model for rough rock joints, *International Journal of Rock Mechanics, Mining Science and Geomechanical Abstract*, **31**, 279–92.

Hatzor, Y. (1993) The block failure likelihood: a contribution to rock engineering in blocky rock masses, *International Journal of Rock Mechanics, Mining Science and Geomechanical Abstracts*, **30**, 1591–7.

Hatzor, Y.H. and Goodman, R.E. (1997) Three dimensional back analysis of saturated rock slopes in discontinuous rock – a case study, *Geotechnique*, **47**, 817–839.

Hencher, S.R. (1995) Interpretation of direct shear tests on rock joints, in *Proceedings of the 35th US Symposium on Rock Mechanics*, Reno 1995, Daemen, J.J.K. and Schultz, R.A. (eds), Balkema, Rotterdam, pp. 99–106.

Hoek, E. and Bray, J.W. (1981) *Rock Slope Engineering*, 3rd edn. Institution of Mining and Metallurgy, London.

Holtz, D.H. and Kovacs, W.D. (1981) *An Introduction To Geotechnical Engineering*, Prentice Hall, Englewood Cliffs, NJ.

Jaeger, J.C. (1971) Friction of rocks and stability of rock slopes, *Geotechnique*, **21**, 97–134.

Ladanyi, B. and Archambault, G. (1970) Simulation of shear behaviour of a jointed rock mass, in *Proceedings of the 11th Symposium on Rock Mechanics*, AIME, New York, pp.105–25.

Ladanyi, B. and Archambault, G. (1977) Shear strength and deformability of filled indented joints, in *International Symposium on the Geotechnics of Structurally Complex Formations*, AGI, Capri, Vol. 2, pp. 317–26.

Patton, F.D. (1966) Multiple modes of shear failure in rock, in *Proceedings of the 1st International Congress of Rock Mechanics*, Lisbon, Vol. 1, pp. 509–13.

Rengers, N. (1970) Influence of surface roughness on the friction properties of rock planes, in *Proceedings of the 2nd International Congress of Rock Mechanics*, Belgrade, Vol. 1, pp. 229–34.

Skempton, A.W. and Petley, D.J. (1967) The strength of structural discontinuities in stiff clays, in *Proceedings of the Geotechnical Conference*, Oslo, Vol. 2, pp. 29–46.

Terzaghi, K. (1962) Stability of steep slopes on hard unweathered rock, *Geotechnique*, **12**, 251–70.

West, T.R. (1996) The effects of positive pore pressure on sliding and toppling of rock blocks with some considerations of intact rock effects, *Environmental and Engineering Geosciences*, **2**, 339–54.

Wittke, W. (1990) *Rock Mechanics – Theory and Applications with Case Histories*, Springer-Verlag, Berlin.